AIAA 2012-5044

Fuel-Efficient Feedback Control of Orbital Motion Around an Irregular-Shaped Asteroid

Tim Winkler,* Matt Hawkins,† Joshua Lyzhoft,‡ and Bong Wie§
Iowa State University, Ames, Iowa 50011-2271

Unmanned probes are the primary technologies used when exploring celestial bodies in our solar system. Unlike with larger bodies such as planets, the dynamical environment around small bodies such as asteroids and comets is difficult to characterize. The gravitational fields are not uniform, and perturbation forces such as solar radiation pressure can be strong enough to destabilize an orbit around an asteroid. There has been research devoted to finding open-loop solutions to stable orbits about small bodies, but the solutions prove to be highly sensitive to the initial conditions. It is shown that a simple feedback control augmented by a disturbance-accomodating filtering can be employed to maintain stable orbital motion about a small body with little ΔV expenditure.

Nomenclature

$\bar{C}_{n,m}, \bar{S}_{n,m}$	Normalized spherical harmonic coefficients of degree n and order m
$\bar{P}_{n,m}$	Normalized Legendre polynomial of degree n and order m
$\mathbf{A}$	State matrix
$\mathbf{B}$	Control input distribution matrix
$\mathbf{K}$	Control gain matrix
$\mathbf{u}$	Control input vector
$\mathbf{w}$	Disturbances
$\mathbf{x}$	State vector
$\mathbf{x_r}$	Reference state vector
$\hat{\mathbf{n}}$	Unit vector
$\mathbf{A}_d$	Disturbance filter state matrix
$\mathbf{B}_d$	Disturbance filter control matrix
$\mathbf{E}_e$	Edge matrix
$\mathbf{F}_f$	Facet matrix
$\mathbf{Q}$	State vector weighting matrix
$\mathbf{R}$	Control vector weighting matrix
$\mathbf{r}_e$	Position vector from the field point to a facet edge
$\mathbf{r}_f$	Position vector from the field point to a polyhedron facet
$\mathbf{T}$	Transformation matrix from spherical to cartesian coordinates

*Graduate Research Assistant, Department of Aerospace Engineering, Iowa State University, 2271 Howe Hall.
†Graduate Research Assistant, Department of Aerospace Engineering, Iowa State University, 2271 Howe Hall.
‡Graduate Research Assistant, Department of Aerospace Engineering, Iowa State University, 2271 Howe Hall.
§Vance Coffman Endowed Chair Professor, Department of Aerospace Engineering, Iowa State University, 2271 Howe Hall.

$\mathbf{x}_d$	Disturbance filter state vector
$\vec{a}$	Absolute acceleration vector
$\vec{g}$	Gravity acceleration vector
$\vec{r}$	Position vector
$\vec{r}_1$	Position vector to facet vertex 1
$\vec{r}_2$	Position vector to facet vertex 2
$\vec{r}_3$	Position vector to facet vertex 3
$\vec{r}_i$	Position vector from the field point to facet vertex i
$\vec{r}_j$	Position vector from the field point to facet vertex j
$\vec{r}_k$	Position vector from the field point to facet vertex k
$C_{n,m}, S_{n,m}$	Spherical harmonic coefficients of degree n and order m
e_{ij}	Edge length between vertex i and j
G	Gravitational constant
L_e	Dimensionless per-edge factor
$P_{n,m}$	Associated Legendre polynomial of degree n and order m
R	Reference radius in spherical harmonics
t	Current time
U	Gravity potential
X	Inertial x-position
x	Body-fixed frame x-position
Y	Inertial y-position
y	Body-fixed frame y-position
Z	Inertial z-position
z	Body-fixed frame z-position

Symbols

α_i	ith filter state along the X-axis
β_i	ith filter state along the Y-axis
γ_i	ith filter state along the Z-axis
λ	Longitude
μ	Gravitational parameter
ω_f	Dimensionless per-facet factor
ω_{xi}	ith frequency component along the X-axis
ω_{yi}	ith frequency component along the Y-axis
ω_{zi}	ith frequency component along the Z-axis
ϕ	Latitude
$\prod$	Normalization factor
σ	Density
τ_x	Filter state to remove bias in X-axis control
τ_y	Filter state to remove bias in Y-axis control
τ_z	Filter state to remove bias in Z-axis control
$\vec{\omega}$	Rotation vector of the body-fixed frame

I. Introduction

Unmanned, robotic probes are the main tools at our disposal for studying asteroid, comets, and planets in our solar system. Of particular interest is to use these probes to explore the smaller bodies such as asteroids or comets. Scientific interest in these objects mainly focuses on what they can tell us about the evolution and diversity of our solar system. Such missions are also invaluable

in the area of asteroid deflection. Given sufficient warning, an observation probe could be sent to a potentially hazardous object. By flying close to the body, detailed images of the surface can be taken as well as readings on the gravitational forces present. Such data can tell us more about the physical makeup of the body, which would help determine the most efficient deflection method.

To enable such a mission, though, requires a thorough understanding of the dynamical environment around such a small body. Relevant perturbation forces in close-proximity operations include the non-uniform gravitational field of the asteroid caused by a non-homogenous mass distribution and solar radiation pressure. The individual or combined effects of these forces has been shown to destabilize orbits, and cause the spacecraft to impact or escape the asteroid.[1] One proposed solution is to hover above the body as was done in the JAXA Hayabusa mission to Itokawa.[2,3] Hovering about a fixed-point above the asteroid, though, would only be appealing if it was desired to land at a particular point on the body. The propellant required could also lead to shorter mission durations, which would limit the scientific return.

In an effort to avoid the requirements of station-keeping, there has been much research devoted to open-loop solutions of orbits about asteroids and comets and their stability bounds.[1,4–11] While it is possible to find orbits that remain stable for great lengths of time, Figure 1 shows how three different orbits with similar initial conditions about the asteroid 433 Eros can produce radically different results. The first orbit begins at a radius of 32.9 km along the inertial X-axis with a velocity equal to that of the local circular. After numerically simulating the orbit for over a week, it remains in a quasi-stable orbit around the body. The second orbit has a radius of 32.8 km also at the local circular velocity, but is shifted 45° from the X-axis. Here the orbit remains about the body for over a week before finally escaping. The third orbit begins at a radius of 27.85 km along the inertial Y-axis with the local circular velocity. The orbit first travels far away from the body twice before impacting. Given the sensitivity of the dynamic environment at asteroids and comets to initial conditions, it is not practical to rely entirely upon open-loop solutions to keep a spacecraft

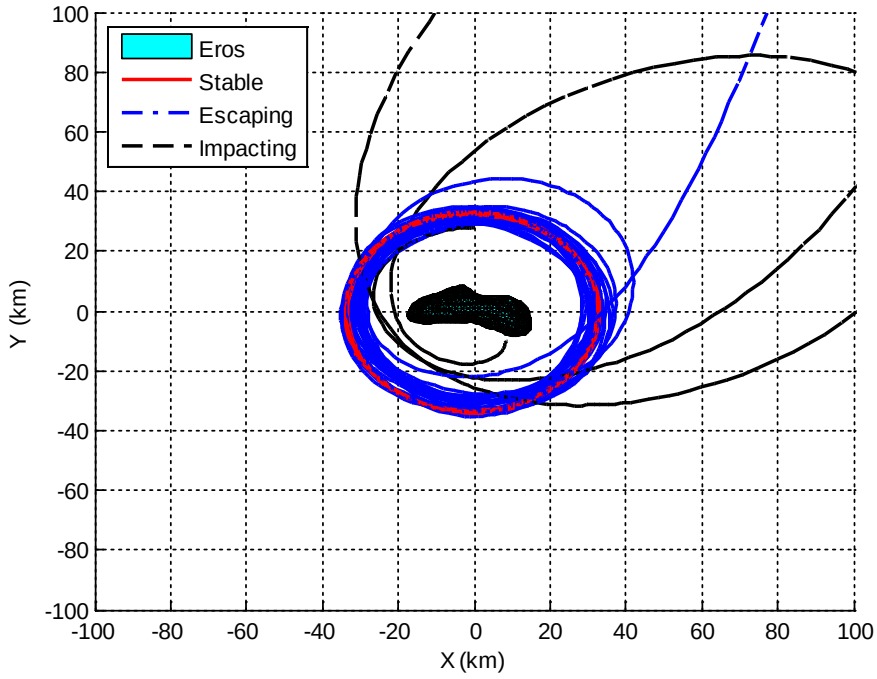

Figure 1. Comparisons of stable, escaping, and impacting orbits around 433 Eros. The coordinate system is an inertial frame fixed at Eros' center of mass with the positive Z-axis along the north pole spin axis. Eros is shown at initial conditions.

in orbit about such a body.

In this paper, the gravitational force of a polyhedron shape model derived by Werner and Scheeres[12] is compared with a 15th order harmonic expansion, and used in simple feedback control logic to command an arbitary orbit about the asteroid 433 Eros. The concept of disturbance accomodating control is then applied in an iterative manner to allow the spacecraft to deviate from the reference trajectory and follow a periodic solution of the nonlinear equations of motion.[13,14] This not only reduces the amount of ΔV required, but also guarantees the spacecraft will remain in orbit about the asteroid for any arbitrary reference orbit.

II. Gravity Models

This section will briefly describe the development of the gravity potential and force equations of both the polyhedron shape model and spherical harmonic expansion used in this paper. A brief derivation of the equations of motion will be given, which will later be used and compared in the results section. The equations for both models will be given in a right-handed coordinate system that is fixed to the rotating asteroid body. This body-fixed frame aligns the positive x-axis along the asteroid's Prime Meridian, and the positive z-axis along the north spin pole. The absolute acceleration of the spacecraft is described by

$$\ddot{\vec{r}} = \ddot{\vec{r}}|_B + 2\vec{\omega} \times \dot{\vec{r}}|_B + \dot{\vec{\omega}} \times \vec{r} + \vec{\omega} \times (\vec{\omega} \times \vec{r}) = \vec{g} + \vec{u} \tag{1}$$

where $\vec{r}$ is the spacecraft position vector, $\vec{g}$ is the gravitational acceleration, $\vec{u}$ is the control acceleration, and $\vec{\omega}$ is the rotation vector of the body-fixed frame (i.e., the angular velocity vector of an asteroid). With the way the coordinate systems are set up, the rotation vector has only one constant component in the positive z-direction. The spacecraft position vector can then be transformed from the body-fixed frame (x, y, z) to the inertial frame (X, Y, Z) as follows

$$\begin{bmatrix} X \\ Y \\ Z \end{bmatrix} = \begin{bmatrix} \cos(\omega t) & -\sin(\omega t) & 0 \\ \sin(\omega t) & \cos(\omega t) & 0 \\ 0 & 0 & 1 \end{bmatrix} \begin{bmatrix} x \\ y \\ z \end{bmatrix} \tag{2}$$

II.A. Polyhedron Gravitation

The polyhedron gravitational model can be advantageous when the gravitating body has a complex, irregular shape. Although computationally slower than using a spherical harmonics expansion, the model is valid anywhere around the body, whereas spherical harmonics is only valid outside of a circumscribing sphere. Here we will show the relevant equations used to simulate the gravitational attraction of a polyhedron. Note that these equations assume a constant density, and that the shape model uses triangular facets. The complete derivation is given by Werner and Scheeres in Ref. 12. The potential function is given as

$$U = \frac{1}{2} G\sigma \sum_{e \in edges} L_e \mathbf{r}_e^T \mathbf{E}_e \mathbf{r}_e - \frac{1}{2} G\sigma \sum_{f \in facets} \omega_f \mathbf{r}_f^T \mathbf{F}_f \mathbf{r}_f \tag{3}$$

where G is the gravitational constant, σ is the density, $\mathbf{r}$ is a vector from a point in space to an edge or facet on the polyhedron, $\mathbf{E}_e$ is a 3×3 edge matrix, L_e is a dimensionless per-edge factor, $\mathbf{F}_f$ is a 3×3 facet matrix, and ω_f is a dimensionless per-facet factor. $\mathbf{E}_e$ and $\mathbf{F}_f$ are given by

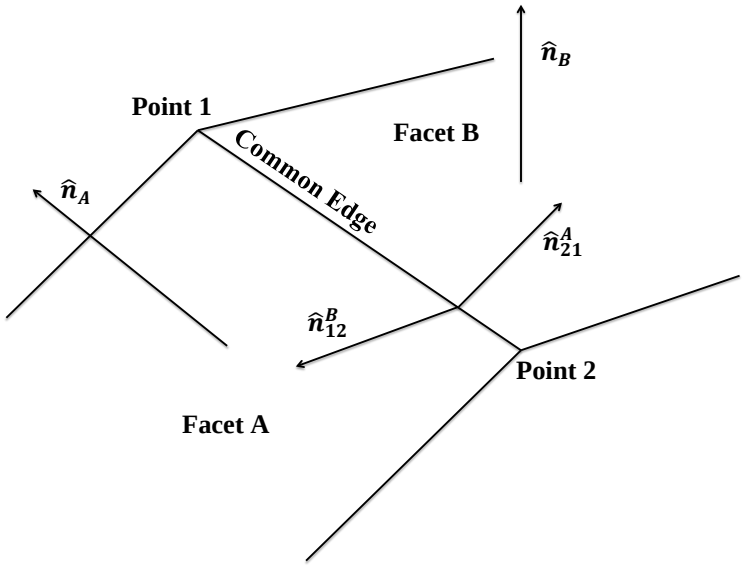

Figure 2. Illustration of the unit facet normal and unit edge normal vectors.

$$\mathbf{E}_e = \hat{\mathbf{n}}_A(\hat{\mathbf{n}}_{21}^A)^T + \hat{\mathbf{n}}_B(\hat{\mathbf{n}}_{12}^B)^T \tag{4}$$

$$\mathbf{F}_f = \hat{\mathbf{n}}_f(\hat{\mathbf{n}}_f)^T \tag{5}$$

where $\hat{\mathbf{n}}_f$, $\hat{\mathbf{n}}_A$, and $\hat{\mathbf{n}}_B$ are outward facing unit normal column vectors and $\hat{\mathbf{n}}_{12}^A$ and $\hat{\mathbf{n}}_{21}^B$ are outward facing edge unit normal column vectors. A graphical illustration of these unit vectors is shown in Figure 2. For a coordinate system, whose origin lies within the polyhedron, the outward facing normal vector can be calculated using

$$\vec{n}_f = (\vec{r}_2 - \vec{r}_1) \times (\vec{r}_3 - \vec{r}_2) = \vec{r}_1 \times \vec{r}_2 + \vec{r}_2 \times \vec{r}_3 + \vec{r}_3 \times \vec{r}_1 \tag{6}$$

where $\vec{r}_{1,2,3}$ are vectors from the origin to each of the three vertices that define the triangular facet, and $\vec{n}_f$ is the facet normal vector. In computer modeling applications, the vertices that define each facet are stored in a matrix using either a clockwise or counterclockwise rotation. The rotation direction refers to the direction around the facet you would have to travel to find next vertex point. Equation (6) assumes a counterclockwise rotation. For clockwise rotation storage, simply multiply the equation by -1. The outward facing edge normal vectors, also assuming a counterclockwise rotation, are

$$\vec{n}_{12}^f = (\vec{r}_2 - \vec{r}_1) \times \vec{n}_f \tag{7a}$$

$$\vec{n}_{23}^f = (\vec{r}_3 - \vec{r}_2) \times \vec{n}_f \tag{7b}$$

$$\vec{n}_{31}^f = (\vec{r}_1 - \vec{r}_3) \times \vec{n}_f \tag{7c}$$

Next the dimensionless factors L_e and ω_f are given as

$$L_e = \ln \frac{r_i + r_j + e_{ij}}{r_i + r_j - e_{ij}} \tag{8}$$

$$\omega_f = 2\arctan\frac{\vec{r}_i \cdot \vec{r}_j \times \vec{r}_k}{r_i r_j r_k + r_i(\vec{r}_j \cdot \vec{r}_k) + r_j(\vec{r}_k \cdot \vec{r}_i) + r_k(\vec{r}_i \cdot \vec{r}_j)} \tag{9}$$

where $\vec{r}_{i,j,k}$ are vectors from the field point to one of the three vertices on the triangular facet, $r_{i,j,k}$ is the magnitude of the vector, and e_{ij} is the length of the edge connecting $\vec{r}_i$ and $\vec{r}_j$. Note that per facet, there will be one value of ω_f and three for L_e (one for each edge). The gravitational force is then the gradient of the potential in Eq. (3) expressed as

$$\nabla U = -G\sigma \sum_{e \in edges} L_e \mathbf{E}_e \mathbf{r}_e + G\sigma \sum_{f \in facets} \omega_f \mathbf{F}_f \mathbf{r}_f \tag{10}$$

The derivation also leads to a simple method for determining whether or not a field point is outside of the polyhedron by taking the Laplacian of the potential, as follows

$$\nabla^2 U = -G\sigma \sum_{f \in facets} \omega_f \tag{11}$$

The sum of ω_f goes to zero when the field point is located outside of the polyhedron, and 4π inside the polyhedron. This is particularly helpful in knowing during a simulation whether or not a spacecraft remained in orbit about a body, or crashed into the surface without requiring much additional computation. Equation (11), however, will not provide any information if the spacecraft escaped the gravitational field of the body. This can only be determined by analyzing the results after a simulation.

II.B. Spherical Harmonics

A more classical approach to gravity modeling is to use spherical harmonics. Although reliable to model gravity for orbiting missions, the equations are only valid outside of a circumscribing sphere around the body. The potential function in spherical harmonics can be expressed as a double summation involving the associated Legendre polynomials, $\mathrm{P}_{n,m}$, and the harmonic coefficients, $\mathrm{C}_{n,m}$ and $\mathrm{S}_{n,m}$[15]

$$U = \frac{\mu}{r}\sum_{n=0}^{\infty}\sum_{m=0}^{n}\left(\frac{R}{r}\right)^n P_{n,m}[\sin(\phi)]\{C_{n,m}\cos(m\lambda) + S_{n,m}\sin(m\lambda)\} \tag{12}$$

$$P_{n,m}[\sin(\phi)] = \frac{1}{2^n n!}(1-\sin^2(\phi))^{m/2}\frac{d^{n+m}}{d\sin(\phi)^{n+m}}(\sin^2(\phi)-1)^n \tag{13}$$

where μ is the gravitational parameter, R is the reference radius of the circumscribing sphere, ϕ is the latitude, and λ is the longitude. Figure 3 shows how ϕ and λ relate to the body-fixed frame. It should be noted that all $\mathrm{S}_{n,0}$ equal zero, and $\mathrm{C}_{0,0}$ is one. Should the coordinate system have its origin at the attracting body's center of mass, the coefficients $\mathrm{C}_{1,0}$, $\mathrm{C}_{1,1}$, and $\mathrm{S}_{1,1}$ are all zero. In such a case, Eq. (12) can be expressed as

$$U = \frac{\mu}{r}[1 + \sum_{n=2}^{\infty}\sum_{m=0}^{n}\left(\frac{R}{r}\right)^n P_{n,m}[\sin(\phi)]\{C_{n,m}\cos(m\lambda) + S_{n,m}\sin(m\lambda)\} \tag{14}$$

For our purposes we will use the more general case given in Eq. (12) to calculate the gradient of the potential in spherical coordinates before converting to a cartesian coordinate system to determine the gravitational acceleration vector, as follows:

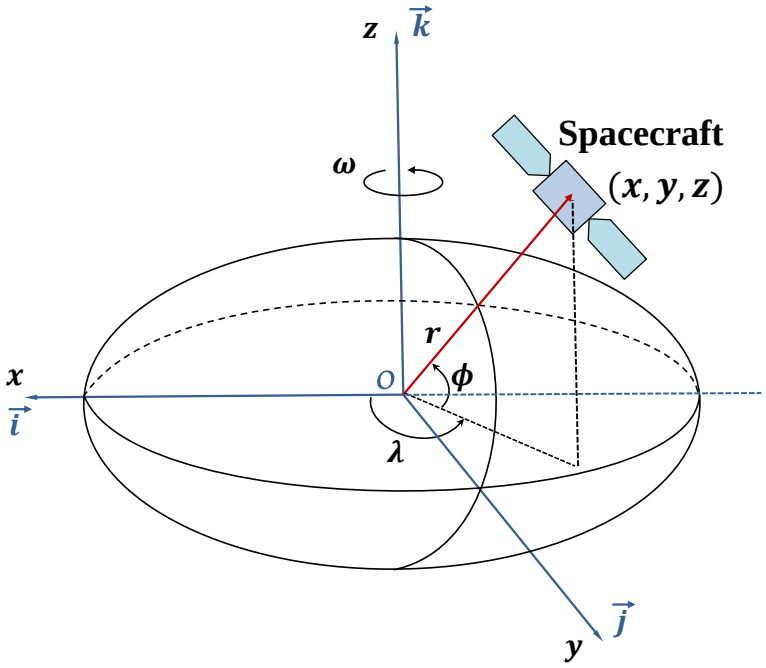

Figure 3. Illustration of the spherical coordinate system with respect to the body-fixed frame.

$$\vec{g} = \frac{\partial U}{\partial r}\hat{e}_r + \frac{1}{r}\frac{\partial U}{\partial \phi}\hat{e}_\phi + \frac{1}{r\cos(\phi)}\frac{\partial U}{\partial \lambda}\hat{e}_\lambda \tag{15}$$

where

$$\frac{\partial U}{\partial r} = -\frac{\mu}{r}\sum_{n=0}^{\infty}\sum_{m=0}^{n}\left(\frac{R}{r}\right)^n (n+1)P_{n,m}[\sin(\phi)]\{C_{n,m}\cos(m\lambda) + S_{n,m}\sin(m\lambda)\} \tag{16a}$$

$$\frac{\partial U}{\partial \phi} = \frac{\mu}{r}\sum_{n=0}^{\infty}\sum_{m=0}^{n}\left(\frac{R}{r}\right)^n \{P_{n,m+1}[\sin(\phi)] - m\tan(\phi)P_{n,m}[\sin(\phi)]\}\{C_{n,m}\cos(m\lambda) + S_{n,m}\sin(m\lambda)\} \tag{16b}$$

$$\frac{\partial U}{\partial \lambda} = \frac{\mu}{r}\sum_{n=0}^{\infty}\sum_{m=0}^{n}\left(\frac{R}{r}\right)^n mP_{n,m}[\sin(\phi)]\{S_{n,m}\cos(m\lambda) - C_{n,m}\sin m\lambda\} \tag{16c}$$

The gravitational acceleration vector can then be converted from spherical coordinates to the body-fixed frame using the following transformation matrix

$$\mathbf{T} = \begin{bmatrix} \cos(\phi)\cos(\lambda) & -\sin(\phi)\cos(\lambda) & -\sin(\lambda) \\ \cos(\phi)\sin(\lambda) & -\sin(\phi)\sin(\lambda) & \cos(\lambda) \\ \sin(\phi) & \cos(\phi) & 0 \end{bmatrix} \tag{17}$$

The derivation above applies only in the case when the harmonic coefficients are not normalized. Oftentimes the coefficients will be given as normalized values on the account of the gravitational

coefficients becoming very small as the degree and order get large. In some computers, this would introduce truncation errors so normalization becomes necessary to prevent inaccuracy. A common method of normalization is

$$\prod_{n,m} = \sqrt{\frac{(n+m)!}{(n-m)!k(2n+1)}} \tag{18}$$
$$k = 1 \quad if \quad m = 0$$
$$k = 2 \quad if \quad m \neq 0$$

$$\bar{S}_{n,m} = \prod_{n,m} S_{n,m} \qquad \bar{C}_{n,m} = \prod_{n,m} C_{n,m} \qquad \bar{P}_{n,m} = \frac{P_{n,m}}{\prod_{n,m}} \tag{19}$$

It is important to remember to normalize the Legendre polynomials as well when using normalized coefficients because their product must remain the same (i.e. $\bar{C}_{n,m}\bar{P}_{n,m} = C_{n,m}P_{n,m}$ and $\bar{S}_{n,m}\bar{P}_{n,m} = S_{n,m}P_{n,m}$)

III. State-Feedback Control

Now that models for the gravity field of the body have been developed, we will consider control accelerations for feedback control of orbital motion around an irregular-shaped asteroid.

III.A. PD Control

Proportional-derivative (PD) control is a common, simple feedback control logic. This type of control attempts to minimize the error between a measured variable and a reference value by feeding back the difference multiplied by some controller gain. To implement this control, we first express the equations of motion in state space form. As the gravitational terms are highly nonlinear, we include them as disturbances ($\mathbf{w}$) and have a simple dynamical model as

$$\dot{\mathbf{x}} = \mathbf{A}\mathbf{x} + \mathbf{B}\mathbf{u} + \mathbf{w} \tag{20}$$

$$\mathbf{x} = \begin{bmatrix} X \\ Y \\ Z \\ \dot{X} \\ \dot{Y} \\ \dot{Z} \end{bmatrix}, \quad \mathbf{u} = \begin{bmatrix} u_x \\ u_y \\ u_z \end{bmatrix}, \quad \mathbf{A} = \begin{bmatrix} 0 & 0 & 0 & 1 & 0 & 0 \\ 0 & 0 & 0 & 0 & 1 & 0 \\ 0 & 0 & 0 & 0 & 0 & 1 \\ 0 & 0 & 0 & 0 & 0 & 0 \\ 0 & 0 & 0 & 0 & 0 & 0 \\ 0 & 0 & 0 & 0 & 0 & 0 \end{bmatrix}, \quad \mathbf{B} = \begin{bmatrix} 0 & 0 & 0 \\ 0 & 0 & 0 \\ 0 & 0 & 0 \\ 1 & 0 & 0 \\ 0 & 1 & 0 \\ 0 & 0 & 1 \end{bmatrix}$$

As was mentioned, PD control also requires a reference trajectory, described by

$$X_r(t) = A_x \cos(\omega_x t) \tag{21a}$$
$$Y_r(t) = A_y \sin(\omega_y t) \tag{21b}$$
$$Z_r(t) = A_z \sin(\omega_z t) \tag{21c}$$
$$\dot{X}_r(t) = -A_x\omega_x \sin(\omega_x t) \tag{21d}$$
$$\dot{Y}_r(t) = A_y\omega_y \cos(\omega_y t) \tag{21e}$$
$$\dot{Z}_r(t) = A_z\omega_z \cos(\omega_z t) \tag{21f}$$

where A_x, A_y, and A_z are the amplitudes of the reference trajectory along the X, Y, and Z axes respectively.

For a system described by Eq. (20), with an arbitrary system matrix $\mathbf{A}$, the control can be expressed as

$$\mathbf{u} = -\mathbf{K}(\mathbf{x} - \mathbf{x_r}) \tag{22}$$

where $\mathbf{K}$ is the control gain matrix to be determined, and $\mathbf{x}_r$ is the reference state vector. One way of finding this gain matrix is using a linear quadratic regulator (LQR) method.[13,14] The LQR method works by selecting a $\mathbf{K}$ that minimizes the following performace index

$$J = \frac{1}{2}\int_0^\infty (\mathbf{x}^T\mathbf{Q}\mathbf{x} + \mathbf{u}^T\mathbf{R}\mathbf{u})dt \tag{23}$$

where $\mathbf{Q}$ and $\mathbf{R}$ are user-chosen weighting matrices. Once selected, the control gain matrix $\mathbf{K}$ is obtained as

$$\mathbf{K} = \mathbf{R}^{-1}\mathbf{B}^T\mathbf{X} \tag{24}$$

where $\mathbf{X}$ is the symmetric positive semidefinite solution of the algebraic Riccati equation (ARE)

$$\mathbf{A}^T\mathbf{X} + \mathbf{X}\mathbf{A} - \mathbf{X}\mathbf{B}\mathbf{R}^{-1}\mathbf{B}^T\mathbf{X} + \mathbf{Q} = 0 \tag{25}$$

For a unique solution of $\mathbf{X}$ to exist, four conditions must be met:

1. $\mathbf{Q}$ must be symmetric and positive semidefinite;
2. $\mathbf{R}$ must be symmetric and positive definite;
3. the pair $(\mathbf{A}, \mathbf{B})$ must be controllable (stabilizable);
4. the pair $(\mathbf{A}, \sqrt{\mathbf{Q}}^T\sqrt{\mathbf{Q}})$ must be observable (detectable).

MATLAB is capable of solving the ARE for $\mathbf{K}$ via the command *lqr*.

III.B. Disturbance-Accommodating Control

Disturbance-rejection or disturbance-accommodation control is a technique which can be used to reduce the control effort in the presence of persistent disturbances (Refs. 13 and 14). It works by eliminating parts of the control acceleration, and allows the spacecraft to follow a trajectory that is closer to a natural periodic solution of the nonlinear equations of motion. As we are forcing the spacecraft to follow a particular reference orbit, the nonlinear gravitational effects can cause constant or periodic disturbances, which require a higher control magnitude to cancel out. Since these disturbances cannot be accurately modeled beforehand, we use an iterative method for designing a disturbance-accommodating controller. This method allows the spacecraft to deviate from the reference trajectory and follow one that requires less ΔV.

When first orbiting the gravitating body with only PD control, there exist certain frequency components in the free orbit, that need to be consistently damped out via the control acceleration. These components can be found by examining an FFT (Fast Fourier Transform) plot of the control commands along each axis. Once the spectral components have been indentified, we can design periodic disturbance-accommodation filters of the form

$$\ddot{\alpha}_i + \omega_{xi}^2 \alpha_i = u_x \tag{26a}$$
$$\ddot{\beta}_i + \omega_{yi}^2 \beta_i = u_y \tag{26b}$$
$$\ddot{\gamma}_i + \omega_{zi}^2 \gamma_i = u_z \tag{26c}$$

where ω_{xi}, ω_{yi}, and ω_{zi} represent the ith frequency component in each axis. For constant disturbances, the filters take the form of

$$\dot{\tau}_x = u_x \tag{27a}$$
$$\dot{\tau}_y = u_y \tag{27b}$$
$$\dot{\tau}_z = u_z \tag{27c}$$

where τ_x, τ_y, and τ_z are the filter states necessary to remove any bias in the control acceleration.

The disturbance-accommodation filter can include as many frequencies as are present in the FFT plots. The filter can then be described in state space form

$$\dot{\mathbf{x}}_d = \mathbf{A}_d \mathbf{x}_d + \mathbf{B}_d \mathbf{u} \tag{28}$$

where $\mathbf{x}_d$ is the disturbance filter state vector. It should be noted that if a frequency or bias component is not used during the iteration, the corresponding filter state is not included in $\mathbf{x}_d$. The disturbance filter in Eq. (28) can then be augmented to the system in Eq. (20) as follows:

$$\begin{bmatrix} \dot{\mathbf{x}} \\ \dot{\mathbf{x}_d} \end{bmatrix} = \begin{bmatrix} \mathbf{A} & 0 \\ 0 & \mathbf{A}_d \end{bmatrix} \begin{bmatrix} \mathbf{x} \\ \mathbf{x}_d \end{bmatrix} + \begin{bmatrix} \mathbf{B} \\ \mathbf{B}_d \end{bmatrix} \mathbf{u} \tag{29}$$

The LQR method can also be applied to the augmented system in Eq. (29) to determine a control gain matrix, and the control input is then described as.

$$\mathbf{u} = -\mathbf{K} \begin{bmatrix} \mathbf{x} - \mathbf{x}_r \\ \mathbf{x}_d \end{bmatrix} \tag{30}$$

In an iterative design, spectral components are indentified and added to the disturbance filter state in Eq. (28) each time the control is updated. Care must be taken, though, in selecting $\mathbf{Q}$ and $\mathbf{R}$ during these updates as the same weighting matrices might not be valid with the new system, or the choice for $\mathbf{Q}$ and $\mathbf{R}$ can cause the system to not be a minimum. These iterations are necessary as suppressing frequency components in the control can result in different frequency components appearing in the control. Normally these frequency components are some integer combination of the body spin rate and the orbit frequency. After several iterations, a disturbance-accommodating controller can be designed that results in a drastic reduction of ΔV.

IV. Fuel-Efficient Orbit Control around Asteroid Eros

The gravity models described in Section II will now be applied to the special case of 433 Eros, one of the largest near-Earth asteroids. We say special case in that the assumption of constant density in the polyhedron gravity model derivation holds true due to the measured center of mass is

Table 1. Normalized spherical harmonic coefficients up to the fourth order with a reference radius of 16 km.

Order	Degree	$\bar{C}_{n,m}$	$\bar{S}_{n,m}$
1	0	0	0
	1	0	0
2	0	-0.05246	0
	1	0	0
	2	0.08240	-0.02811
3	0	-0.00141	0
	1	0.00406	0.00337
	2	0.00177	-0.00070
	3	-0.01042	-0.01207
4	0	0.01293	0
	1	-0.00010	0.00014
	2	-0.01747	0.00463
	3	-0.00030	-0.00012
	4	0.01746	-0.00911

very close to center of mass assuming an uniform internal structure.[16] Eros is also a prime example of an asteroid with a very irregular shape. As seen in Figure 4, Eros has an elongated shape with the largest dimension being more than twice as long as the smallest dimension, and there is also a large concavity near the middle. The figure also illustrates how the gravitational field varies across the asteroid's surface. Here we see that the gravitational force is strongest in the middle of the asteroid and decreases towards the ends furthest from the center.

Using these two models, we will examine four different scenarios: a prograde and retrograde orbit in the XY-plane, a 45° inclined orbit, and a polar orbit. In each case, the spacecraft will follow a 35 km radius circular reference orbit. It is unlikely that a realistic mission would follow an orbit that is so close to an asteroid, but the irregularities in the gravity field are stronger and more noticeable the closer the spacecraft comes to the body. Being able to orbit closer to the asteroid is not without its advantages, though, as scientists can observe the object in greater detail. For our purposes, it is assumed that all of the states can be measured for feedback control and the thrusters are capable of producing the required control accelerations. Both models assume an asteroid density of 2.67 g/cm^3 and rotation period of 5.27 hours, and the spherical harmonics uses a reference radius of 16 km. Table 1 lists the normalized gravity harmonic coefficients up to the fourth order. Both the shape model and the spherical harmonic coefficients were downloaded from NASA's website of shape and gravity models produced by the NEAR Shoemaker mission.[17]

IV.A. XY-Plane Prograde Orbit

We will first examine a prograde orbit in the XY-plane about the asteroid. The orbit begins on the X-axis at the local circular velocity. The resulting orbit, control accelerations, and FFT plots are given in Figures 5-8. In Figure 7, a quick comparison between the polyhedron model and the harmonics model results show very little difference in the X- and Y-control and a slight bias difference in the Z-control. Integrating these control accelerations results in a ΔV of 21.13 m/s per week with the polyhedron model and 21.37 m/s with the harmonics model. Figure 8 contains the spectral components of the control accelerations. Both models show five noticeable peaks in the X- and Y-control and two in the Z. For the X and Y FFTs, the two highest peaks correspond to the

(a) 3D model of 433 Eros based on NEAR's Laser Rangefinder measurements.

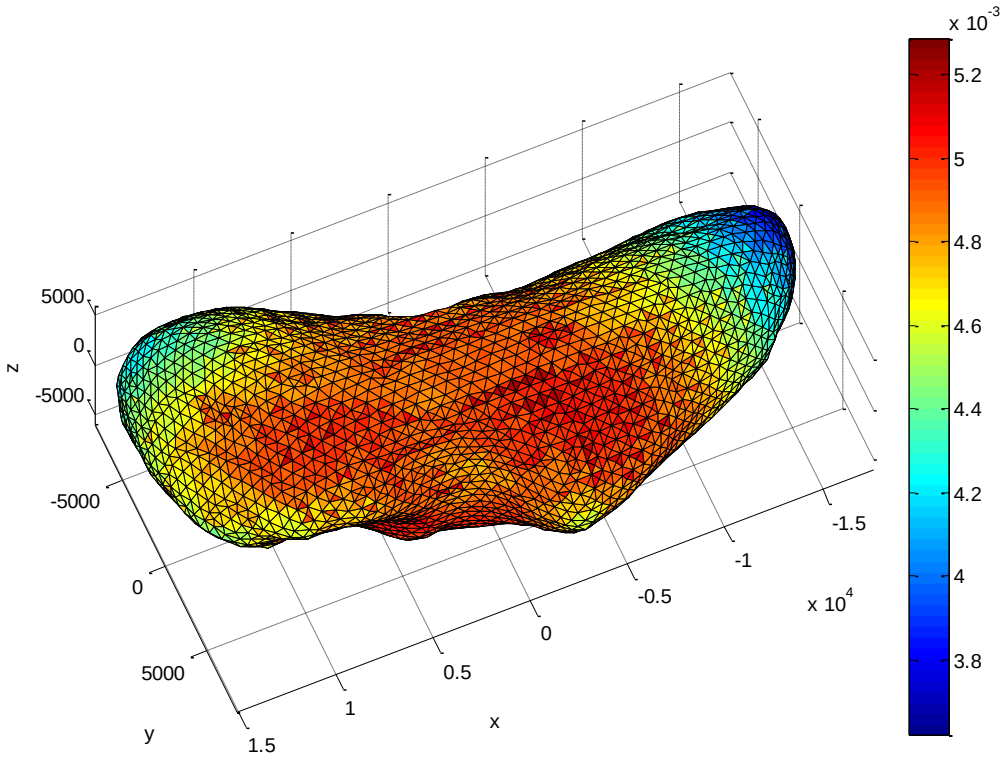

(b) Surface gravitational acceleration from the polyhedron shape model.

Figure 4. Image of 433 Eros derived from NEAR Shoemaker measurements shown next to the plate model used for polyhedron gravity model.

orbit frequency and twice the asteroid rotation frequency minus three times the orbit frequency. Figures 9 and 10 show the results of adding filters of the form in Eq. (26) to each of the prominent frequency components after one iteration. After some initial transients, the control accelerations decrease to a fraction of their former magnitude, and the bias in both Z-controls was completely eliminated. Both models gave a new ΔV requirement of slightly more than 1 m/s per week.

IV.B. XY-Plane Retrograde Orbit

Next we will examine the same orbit except being retrograde instead of prograde. Adding PD control results in an identical ΔV requirement as the prograde case. This would not be obvious by comparing the control acceleration histories in Figures 7 and 11. The Z-axis controls for both retrograde and prograde have about the same amplitude, but the retrograde control oscillates at a higher frequency. On the other hand, the X- and Y-controls for both cases differ greatly from one another both in shape and frequency. This is also reflected in the FFT plots in Figures 8 and 12 as the prograde orbit has less peaks present (5 noticeable peaks in the X and Y as opposed to 6). The largest peak for the retrograde orbit also occurs at a higher frequency than the prograde orbit for each axis control. Adding filters to these frequencies gave a new ΔV requirement of 0.99 m/s per week for the polyhedron model and 0.94 m/s for the harmonic model.

IV.C. 45° Inclined Orbit

Now we will incline the orbit by 45 degrees to command an orbit that is not in any of the coordinate system planes. When left uncontrolled, an orbit of this type will naturally precess about the asteroid. Adding PD control will prevent this precession from happening at the expense of a ΔV of 17.65 m/s per week for the polyhedron model and 17.59 m/s for the harmonics model. In this case, the control accelerations along each axis exhibit the same frequency peaks in the FFT plots, though not necessarily with the same magnitude. Filtering these frequencies allows the spacecraft to be controlled, while also precessing as it would naturally about the asteroid as shown in Figure 16. After applying filters to all the frequencies present in Figure 18, the control accelerations go to nearly zero, and the ΔV requirement is reduced to 0.5 m/s per week for both models.

IV.D. Polar Orbit

Perhaps the most useful orbit to command, in terms of scientific return, would be a polar orbit. Whereas an orbit in the XY-plane would be limited to only viewing parts of the surface in the plane, a polar orbit would be able to view the entire surface due to the spin of the asteroid. Using PD control, we see the most irregular control acceleration history out of the four scenarios (Figure 21). While there is still periodicity, the curves for the in-plane controls (X and Z) are not as smooth flowing for the inclined, prograde, or retrograde orbits. Despite being the most irregular, this orbit requires the least amount of control effort before applying control filters. The polyhedron model requires 16.85 m/s of ΔV per week, and the harmonic model requires 16.36 m/s. For this orbit, we see the most number of large frequencies in the orbital plane appear on one FFT plot (6 total). While the retrograde case does have this same number of frequencies in the FFT plot, most of them are less than half the size of the two largest peaks. Applying filters to each of the frequencies present, reduces the ΔV per week to 0.89 m/s for both models.

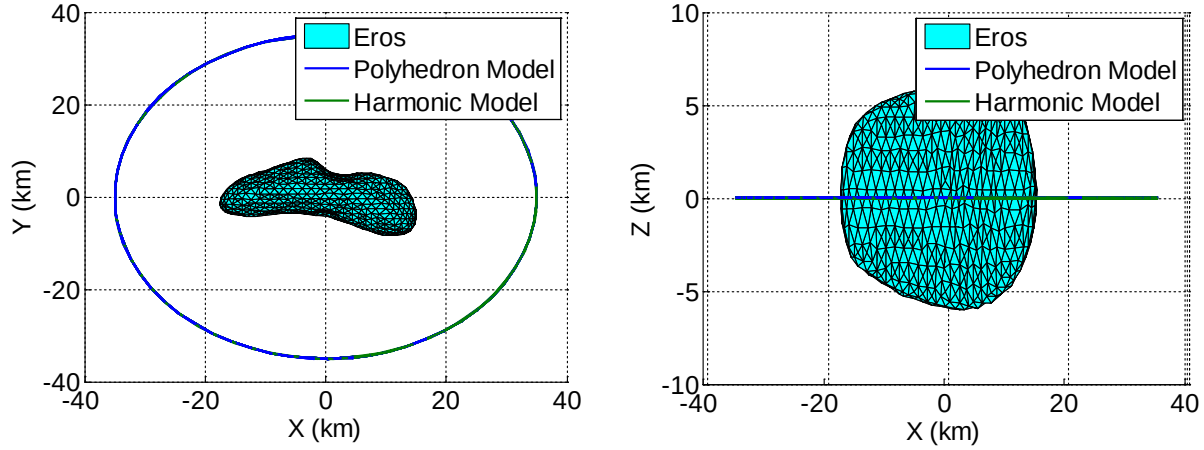

Figure 5. 35 km prograde orbit in the XY-plane with PD control.

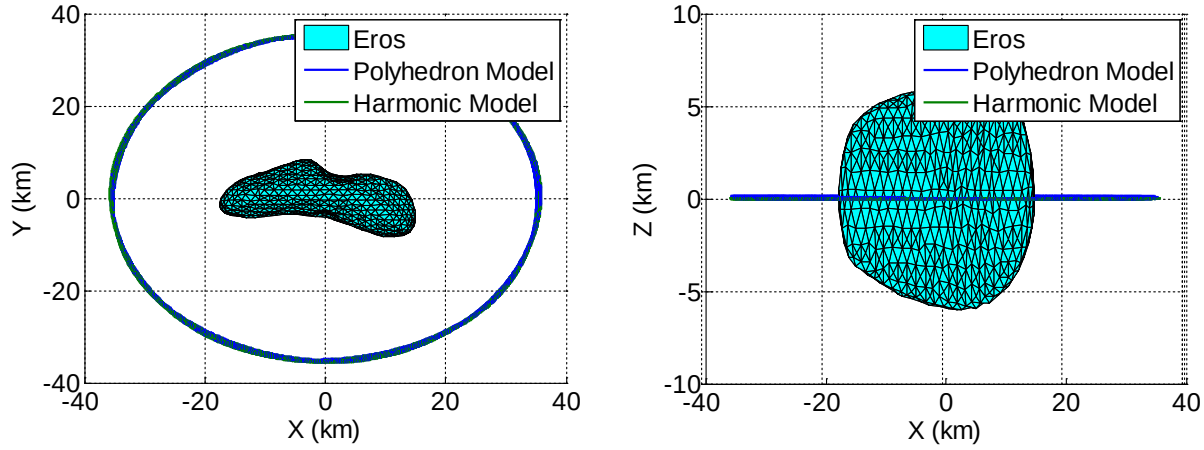

Figure 6. 35 km prograde orbit in the XY-plane with disturbance-accommodating control.

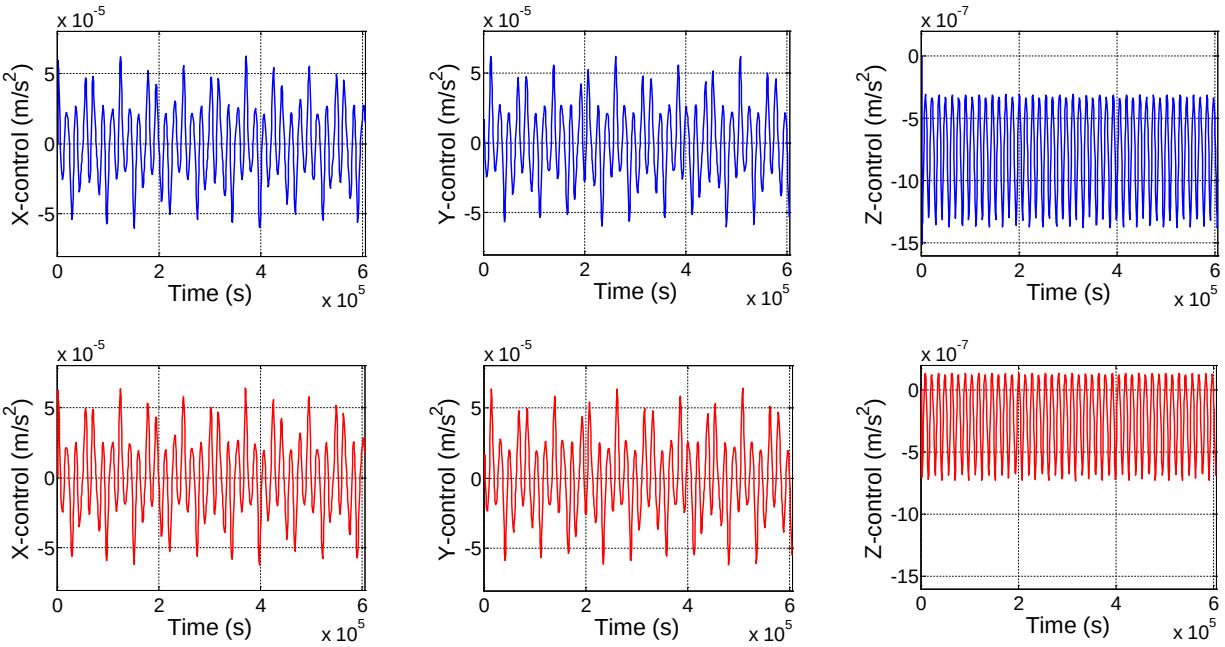

Figure 7. 35 km prograde orbit control acceleration histories with simple PD control. Polyhedron model on top and the harmonics model on bottom.

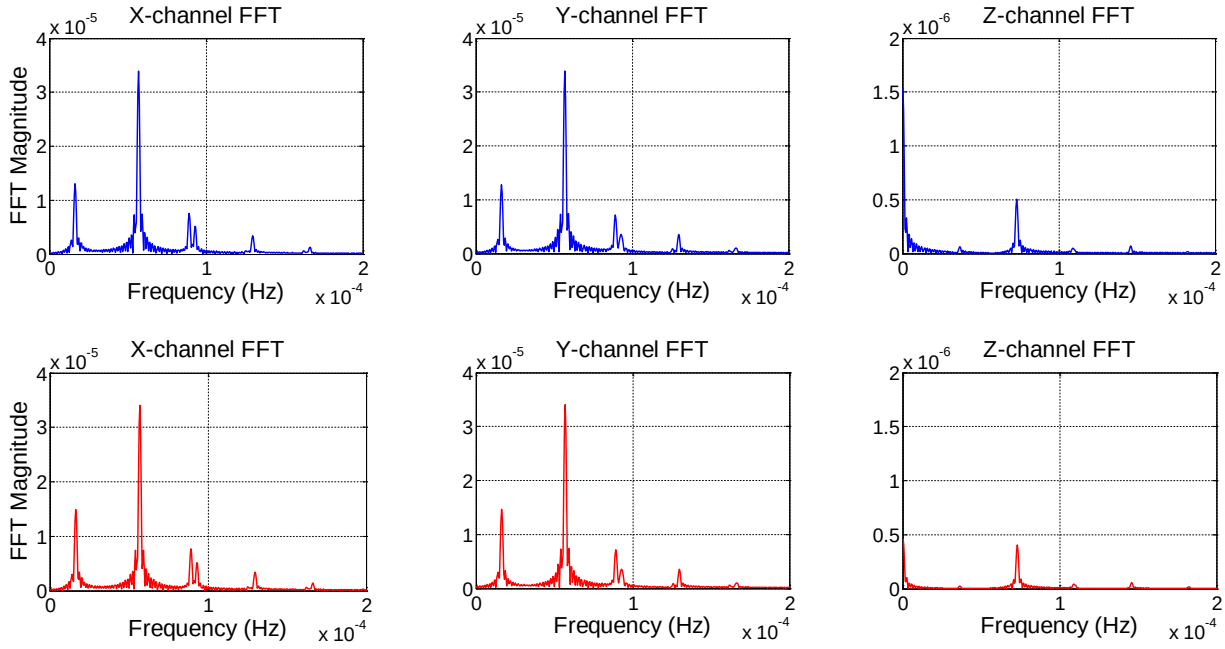

Figure 8. FFT plots of the PD control inputs for the 35 km prograde orbit.

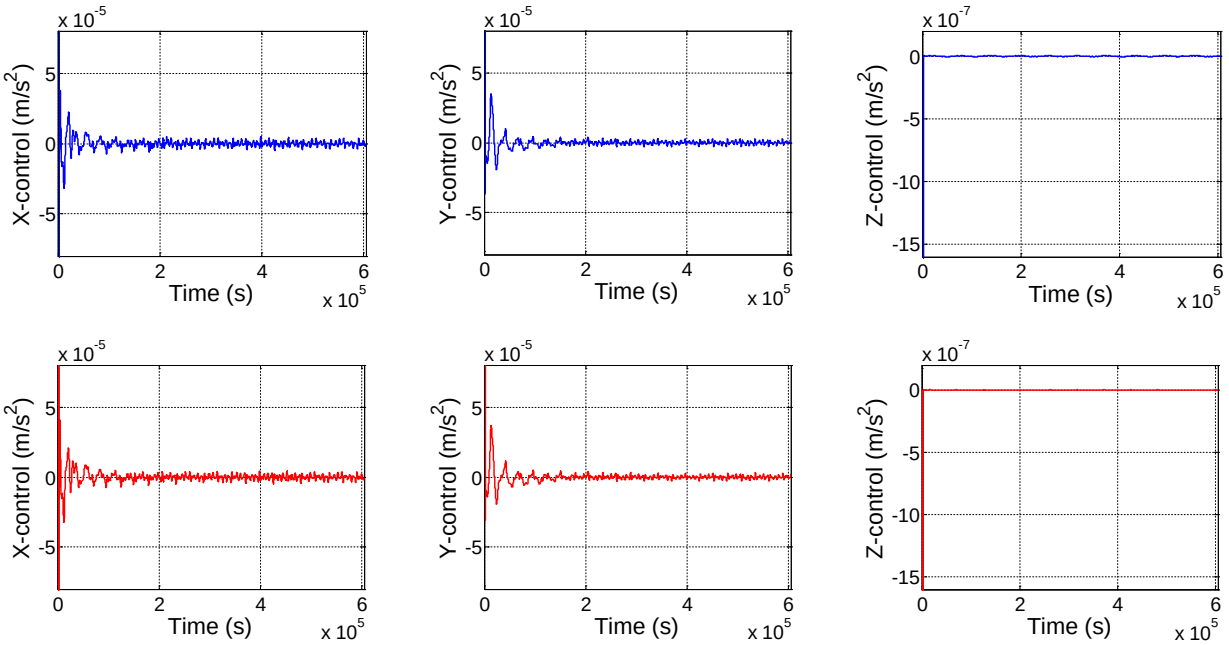

Figure 9. 35 km prograde orbit control acceleration histories with disturbance accommodating control. Polyhedron model on top and harmonics model on bottom.

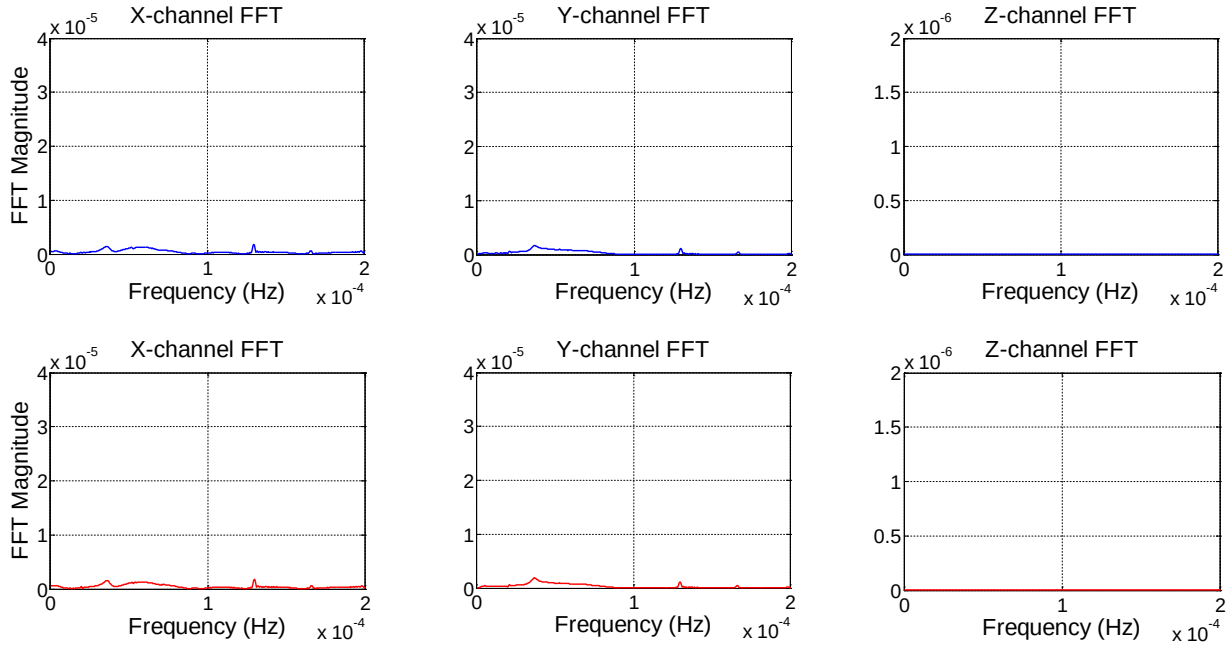

Figure 10. FFT plots of the disturbance accommodating control inputs for the 35 km prograde orbit.

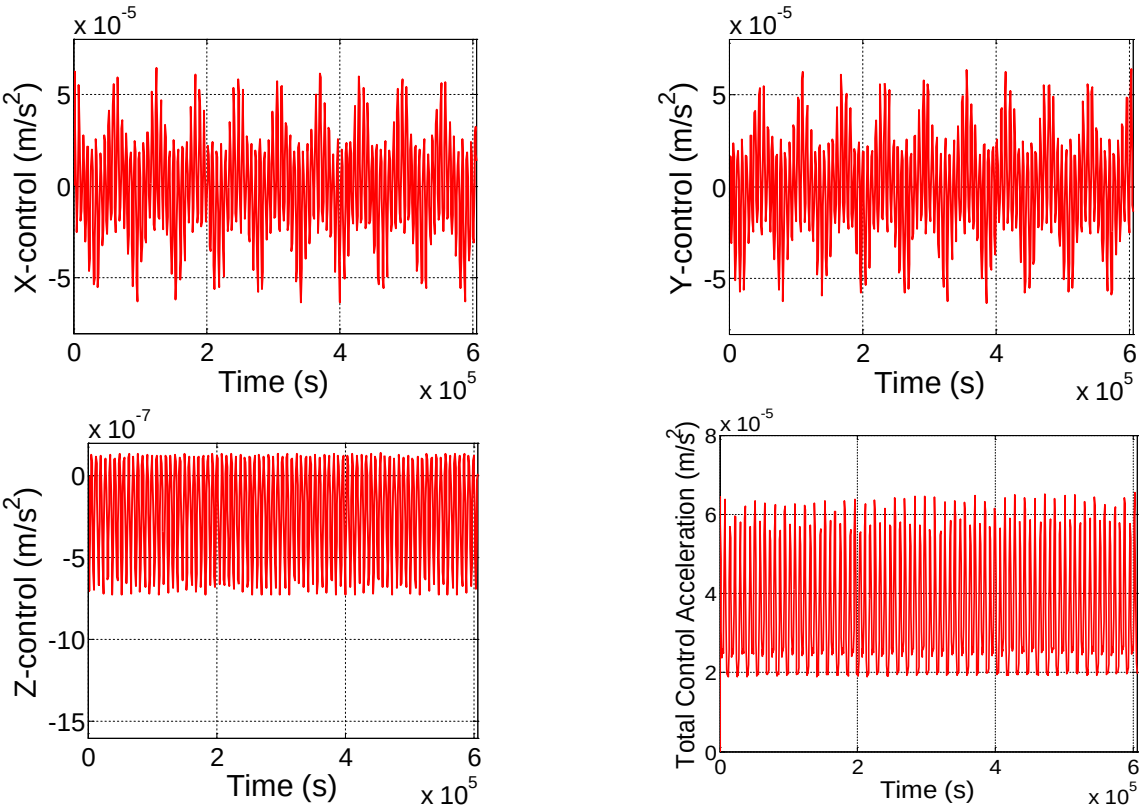

Figure 11. 35 km retrograde orbit control acceleration histories with PD control.

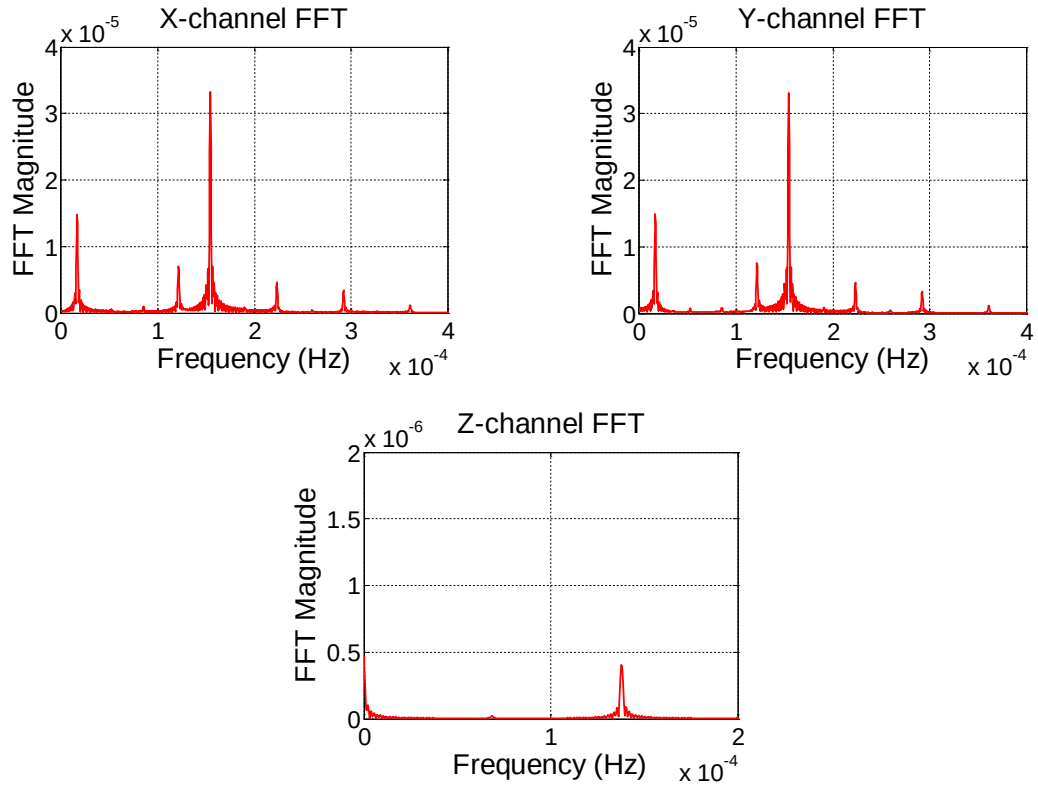

Figure 12. FFT plots of the PD control inputs for the 35 km retrograde orbit.

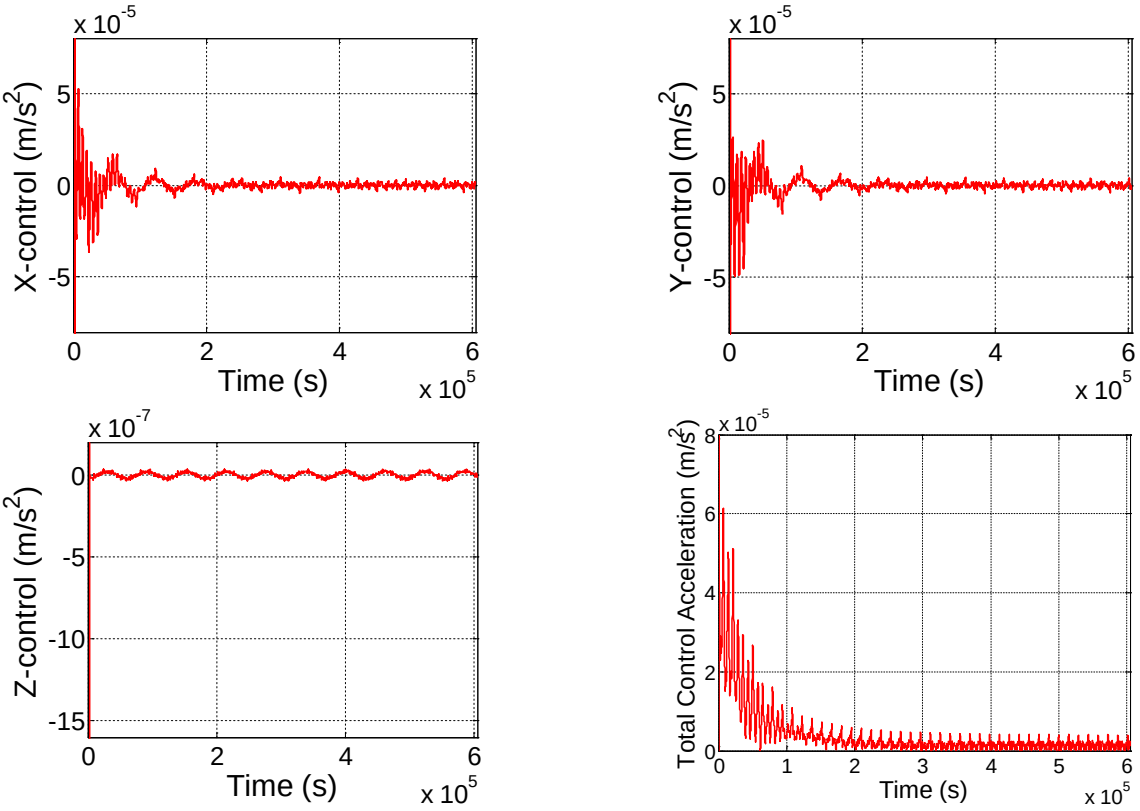

Figure 13. 35 km retrograde orbit control acceleration histories with disturbance accommodating control.

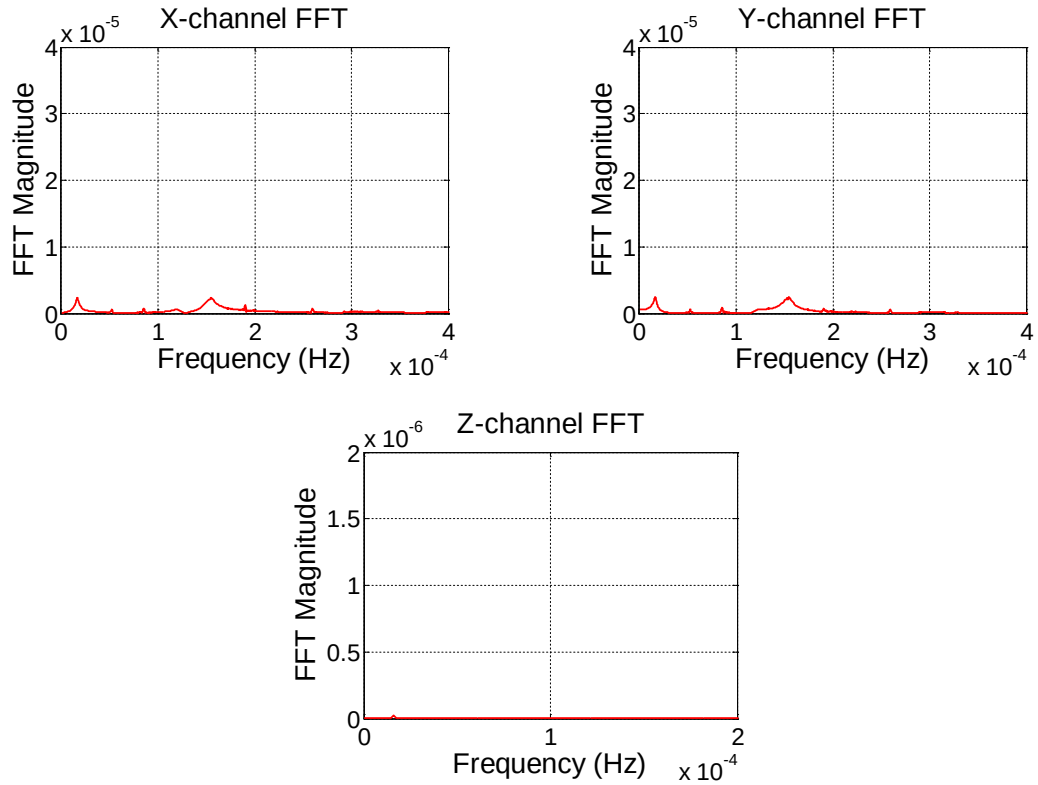

Figure 14. FFT plots of the of the disturbance accommodating control inputs for the 35 km retrograde orbit.

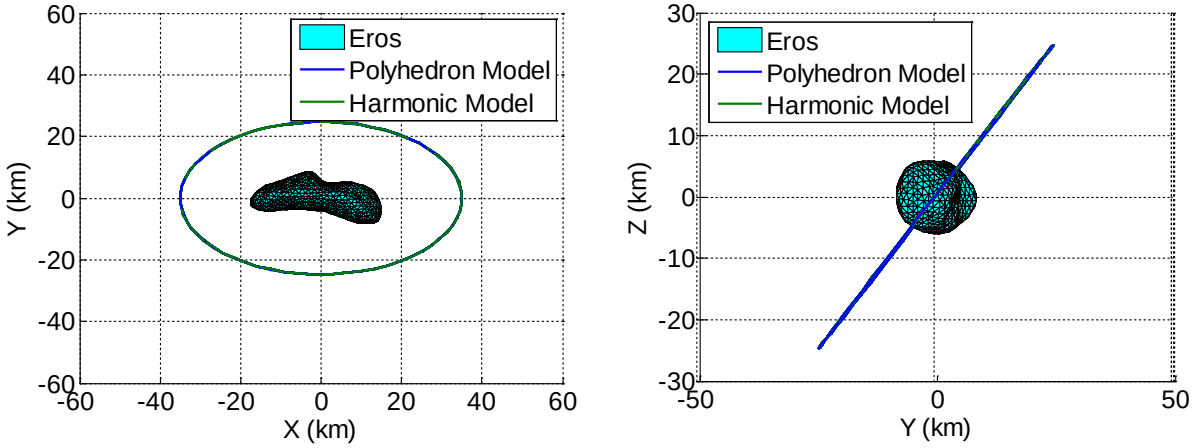

Figure 15. Inclined orbit with PD control.

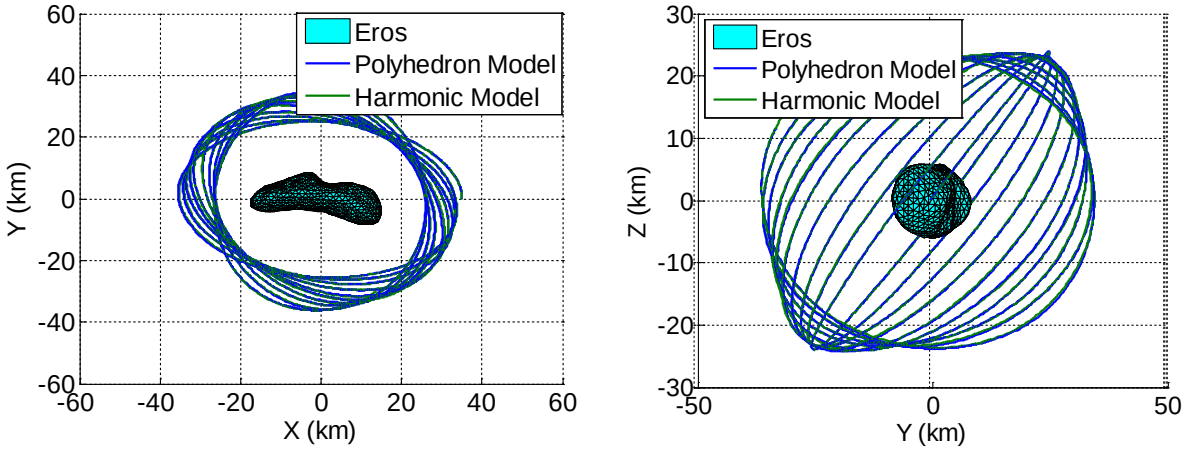

Figure 16. Inclined orbith with disturbance-accommodating control.

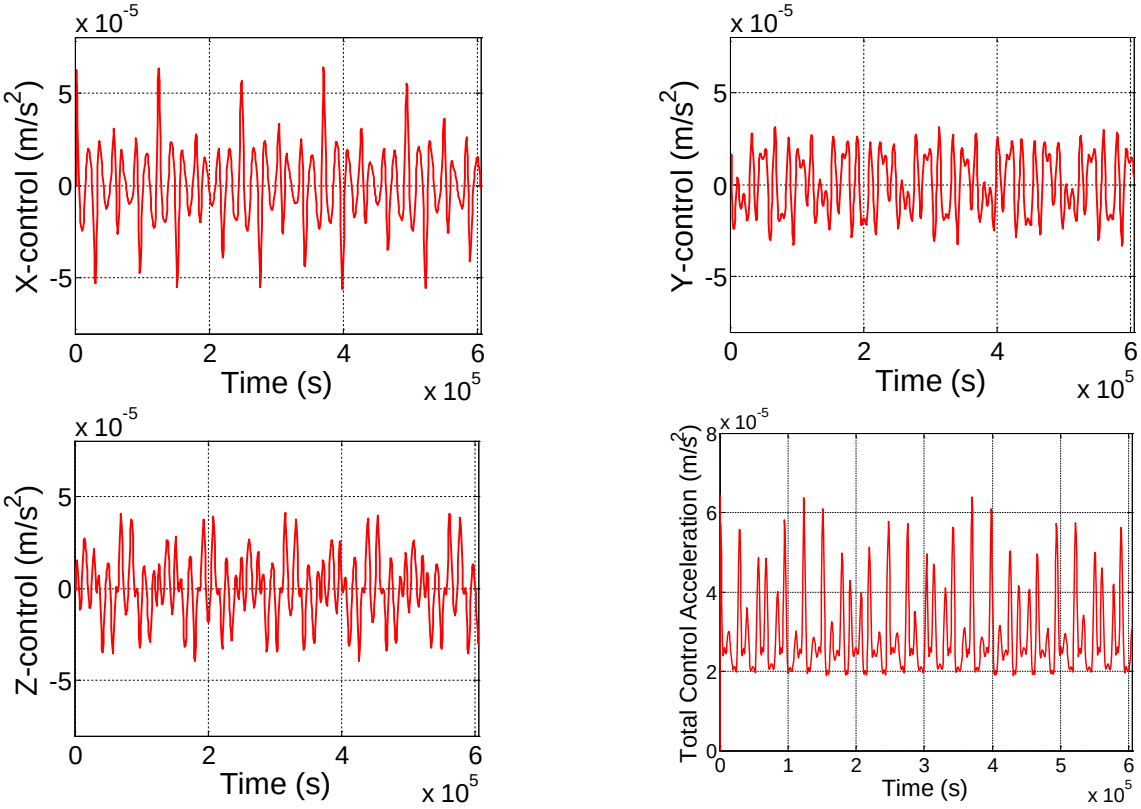

Figure 17. Inclined orbit control acceleration histories with PD control.

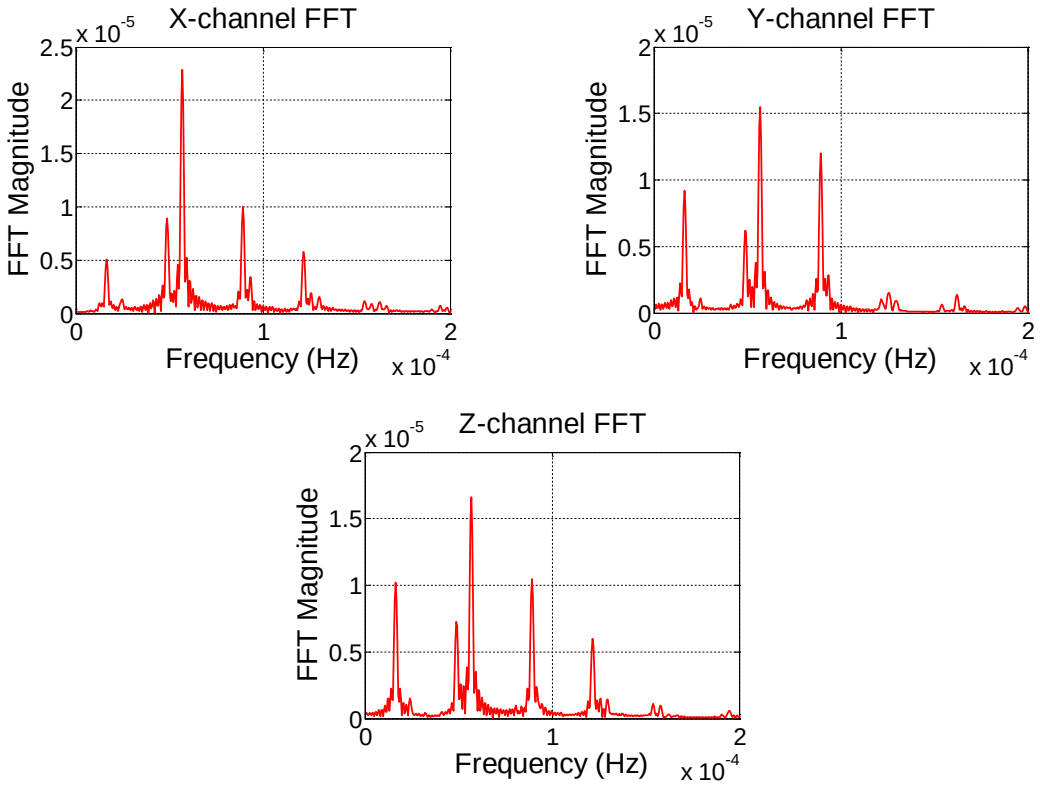

Figure 18. FFT plots of the PD control inputs for the inclined orbit.

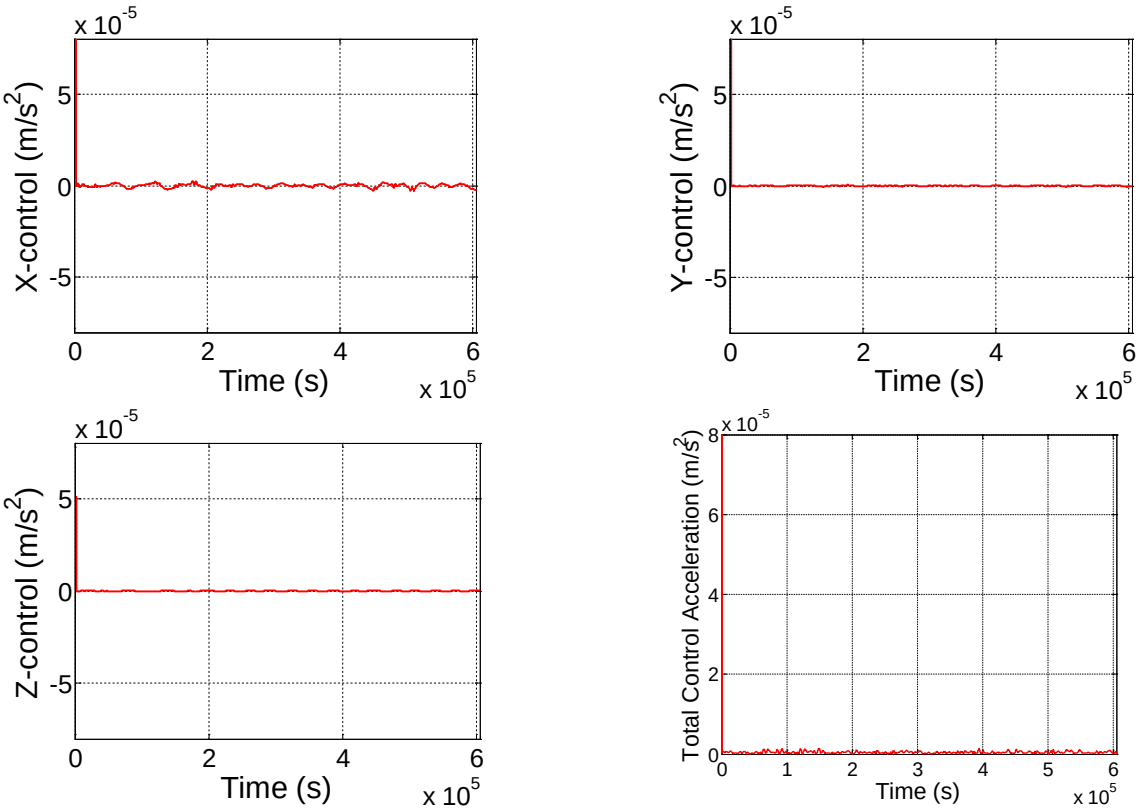

Figure 19. Inclined orbith control acceleration histories with disturbance accommodating control.

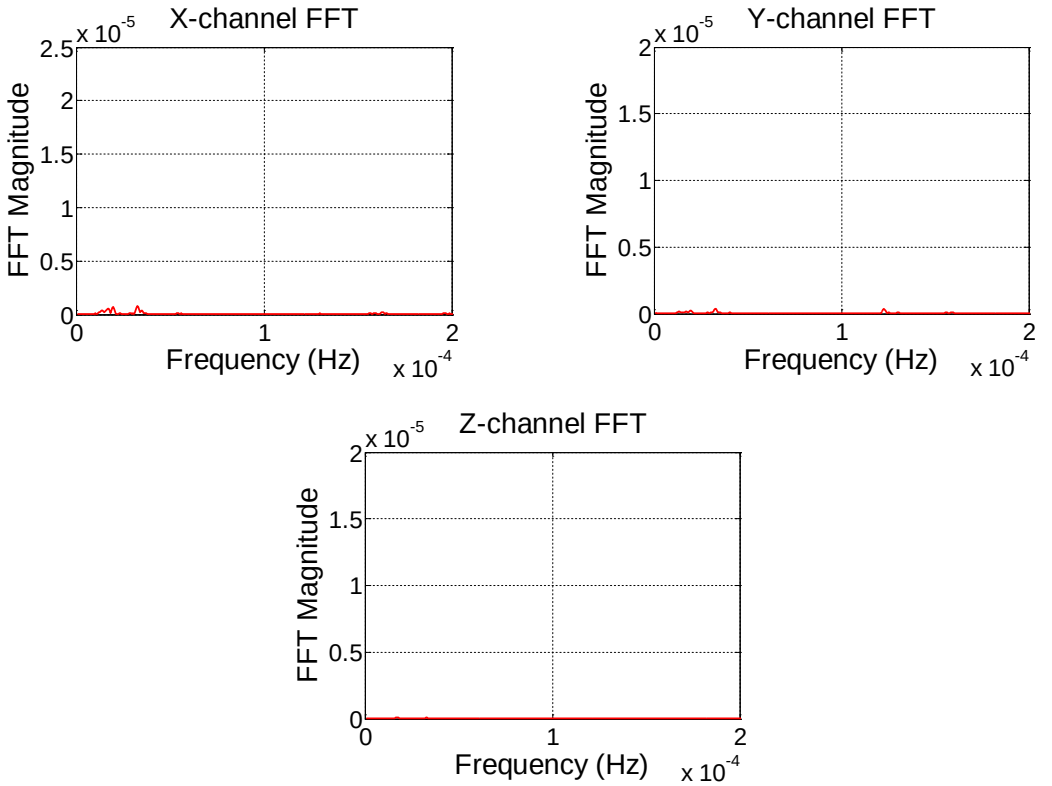

Figure 20. FFT plots of the disturbance accommodating control inputs for the inclined orbits.

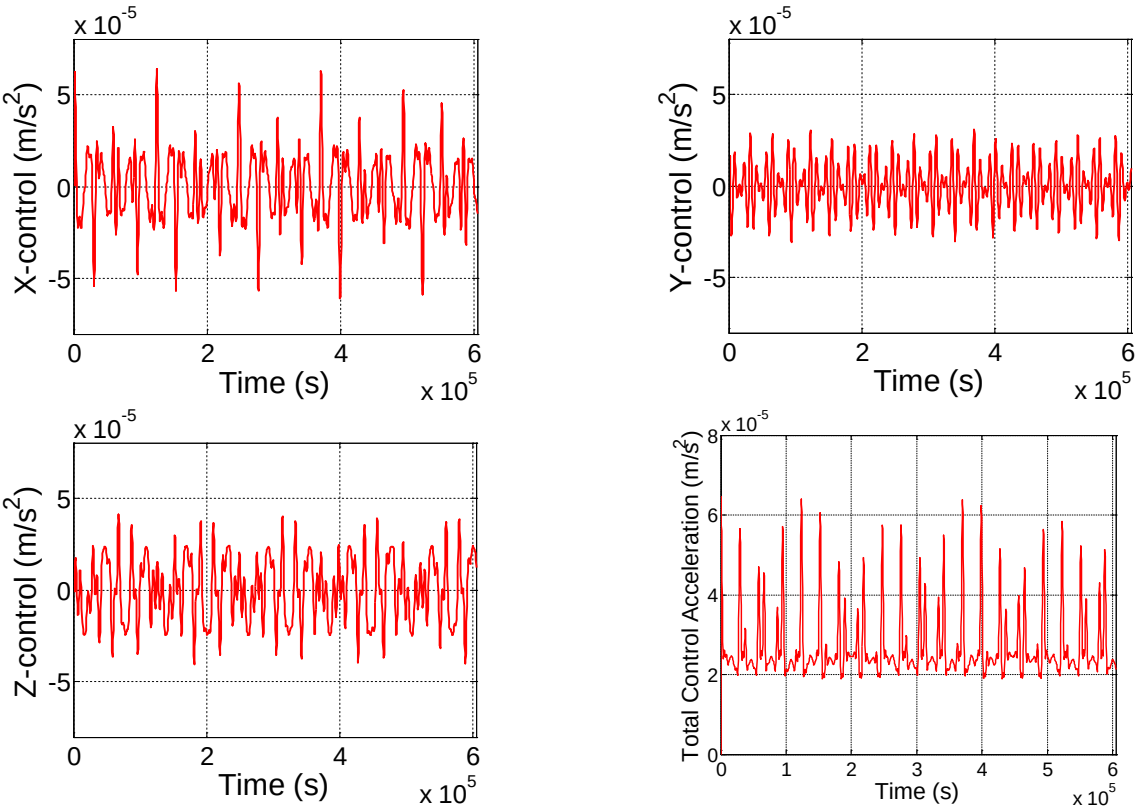

Figure 21. Polar orbit control accelerations with PD control.

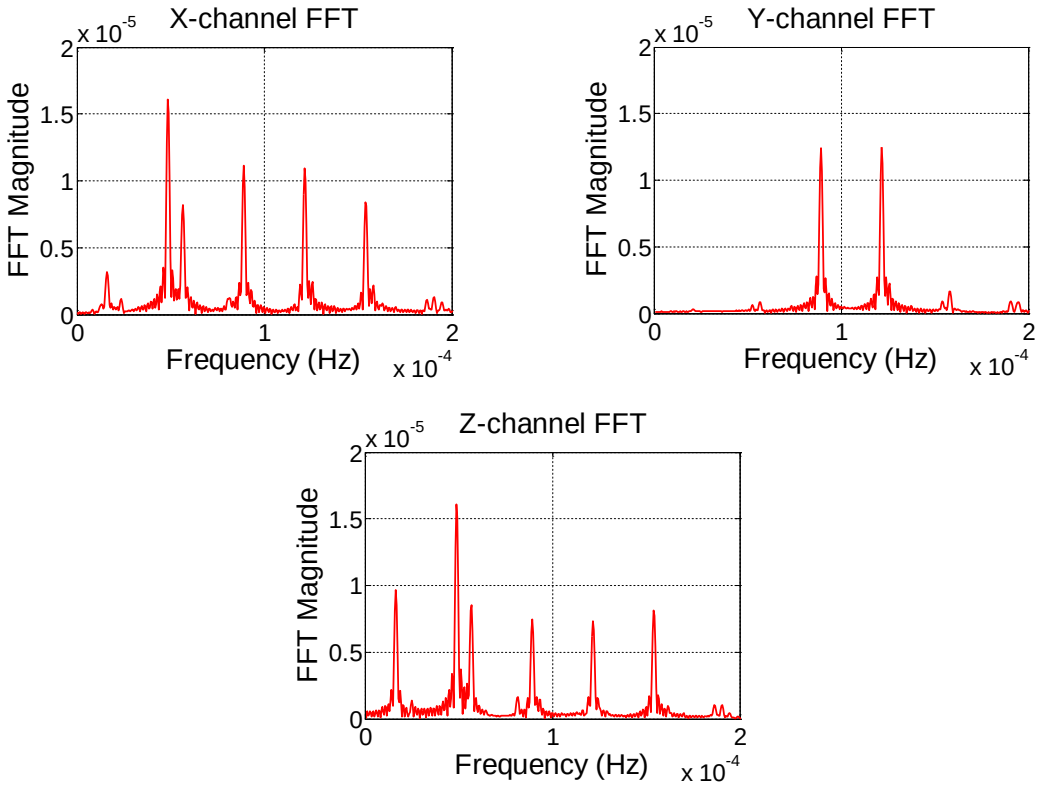

Figure 22. FFT plots of the PD control inputs for the polar orbit.

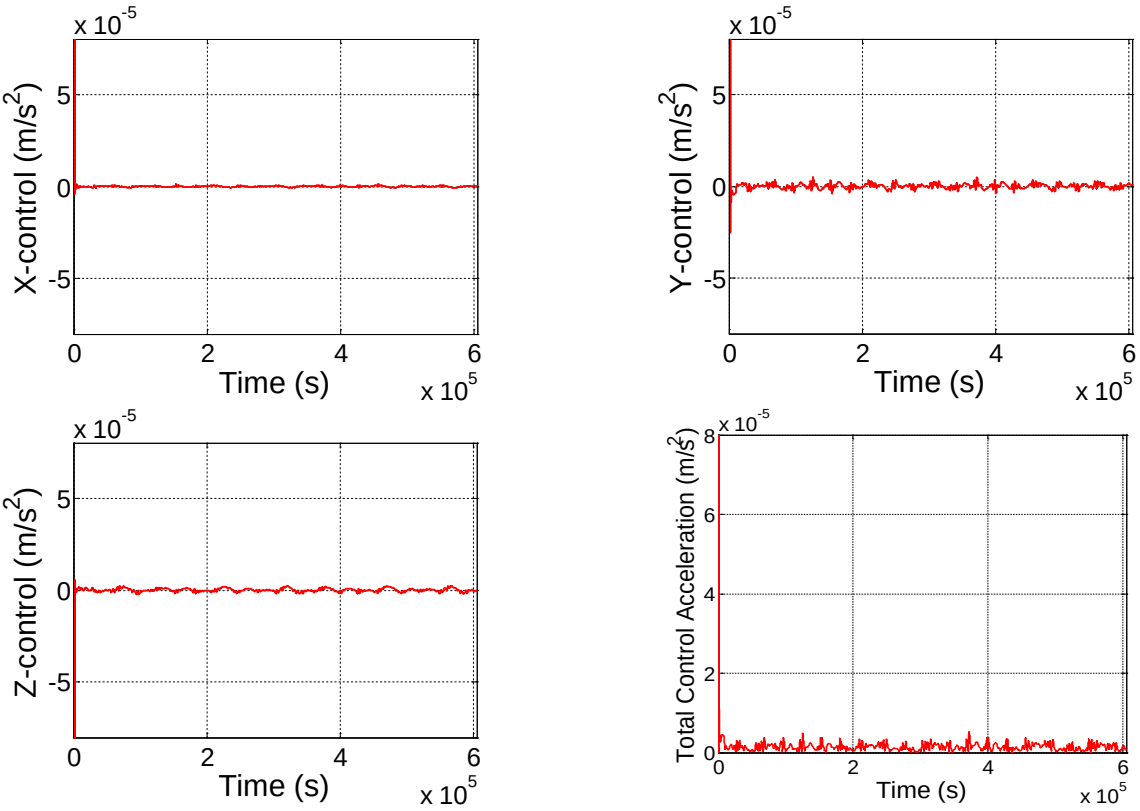

Figure 23. Polar orbit control accelerations with disturbance accommodating control.

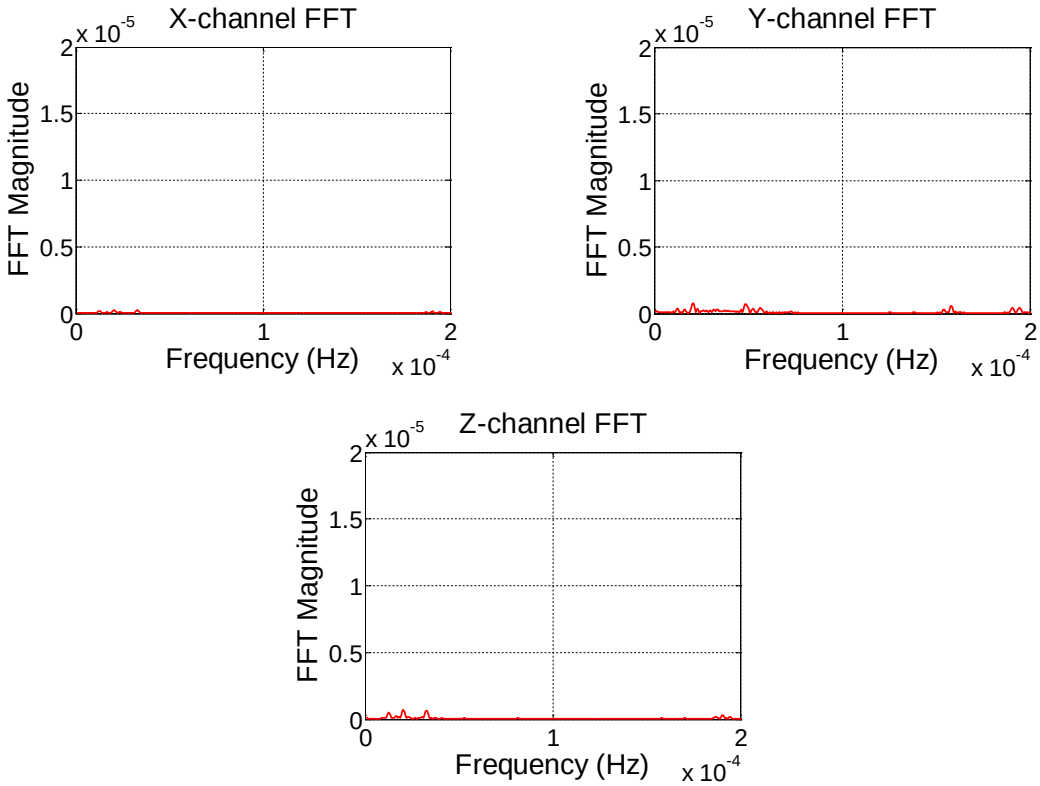

Figure 24. FFT plots of the disturbance accommodating control inputs for the polar orbit.

V. Conclusion

Space agencies around the world will continue to send spacecraft to study small bodies such as asteroids and comets in our solar system. As was shown in this paper, the orbital motions around such bodies are sensitve to the initial conditions and the gravitational environment. Although there has been much study and effort devoted to finding open-loop solutions of stable orbits in such an environment, it is not guaranteed that the spacecraft will always be successfully put into such trajectories. Therefore it was demonstrated that using a simple feedback control combined with a disturbance-accommodating control filter could be implemented to ensure the spacecraft remains in a stable orbit about the body with very little control effort. Another advantage to this control scheme is that, unlike open-loop solutions, prior knowlegde of the body is not required. This is due to the fact that only the control acceleration history is required to know at what frequencies the control filters should be tuned.

References

[1]Scheeres, D. J., "Orbital Mechanics About Small Bodies," *Acta Astronautica*, Vol. 27, 2012, pp. 1-14.

[2]Broschart, S. B. and Scheeres, D. J., "Control of Hovering Spacecraft Near Small Bodies: Application to Asteroid 25143 Itokawa," *Journal of Guidance, Control, and Dynamics*, Vol. 27, No. 2, 2005, pp. 343-354.

[3]Kawaguchi, J., "Hayabusa, Summary of Guidance, Navigation and Control Achievement in its Proximity Phase," *Astrodynamics Specialist Conference*, Keystone, CO, AIAA Paper 2006-6533, Aug. 2006.

[4]Scheeres, D. J., "Dynamics About Uniformly Rotating Tri-Axial Ellipsoids: Applications to Asteroids," *Icarus*, Vol. 110, 1994, pp. 225-238.

[5]Scheeres, D. J., Ostro, S. J., Hudson, R. S., and Werner, R. A., "Orbits Close to Asteroid 4769 Castalia," *Icarus*, Vol. 121, 1996, pp. 67-87.

[6]Scheeres, D. J., Williams, B. G., and Miller, J. K., "Evaluation of the Dynamic Environment of an Asteroid: Applications to 433 Eros," *Journal of Guidance, Control, and Dynamics*, Vol. 23, 2000, pp. 466-475.

[7]Hu, W. and Scheeres, D. J., "Numerical Determination of Stability Regions for Orbital Motion in Uniformly Rotating Second Degree and Order Gravity Fields," *Planetary and Space Science*, Vol. 52, 2004, pp. 685-692.

[8]Hu, W. and Scheeres, D. J., "Periodic Orbits in Rotating Second Degree and Order Gravity Fields," *Chinese Journal of Astronomy and Astrophysics*, Vol. 8, No. 1, 2008, pp.108-118.

[9]Scheeres, D. J., "Satellite Dynamics About Small Bodies: Averaged Solar Radiation Pressure Effects," *Journal of the Astronautical Sciences*, Vol. 47, No. 1, 1999, pp. 25-46.

[10]Scheeres, D. J. and Marzari, F., "Spacecraft Dynamics in the Vicinity of a Comet," *Journal of the Astronautical Sciences*, Vol. 50, No. 1, 2002, pp. 35-52.

[11]Scheeres, D. J., Miller, J. K., and Yeomans, D. K., "The Orbital Dynamics Environment of 433 Eros: A Case Study for Future Asteroid MIssions," InterPlanetary Network Progress Report 42-152, 2003, pp. 1-26.

[12]Werner, R. A. and Scheeres, D. J., "Exterior Gravitation of a Polyhedron Derived and Compared with Harmonic and Mascon Gravitation Representations of Asteroid 4769 Castalia," *Celestial Mechanics and Dynamical Astronomy*, Vol. 65, 1997, pp. 313-344.

[13]Cielaszyk, D. and Wie, B., "New Approach to Halo Orbit Determination and Control," *Journal of Guidance, Control, and Dynamics*, Vol. 19, No. 2, 1996, pp. 266-273.

[14]Wie, B., "Space Vehicle Dynamics and Control, 2nd Edition", American Institute of Aeronautics and Astronautics, 2008.

[15]Vallado, D. A., "Fundamentals of Astrodynamics and Applications, Third Edition," Microcosm Press and Springer, 2007.

[16]Miller, J. K., et al., "Determination of Shape, Gravity, and Rotational State of Asteroid 433 Eros," *Icarus*, Vol. 155, 2002, pp. 3-17.

[17]"NEAR-A-5-COLLECTED-MODELS-V1.0," URL: http://sbn.psi.edu/pds/resource/nearbrowse.html.